25th ABCM International Congress of Mechanical Engineering
October 20-25, 2019, Uberlândia, MG, Brazil

COBEM2019-1487
INFLUENCE OF THE NOZZLE PLATE SPACING ON THE FLOW BEHAVIOR OF A TURBULENT IMPINGING JET

Leticia Fernanda Rabelo Castelo Branco
Danielle Regina da silva Guerra
Antônio Guilherme Barbosa da Cruz
Fábio da Silva Barros
Graduate Program of Mechanical Engineering, PPGEM/ITEC, Federal University of Pará, Belém, Pará, Brazil
leticia.branco@maraba.ufpa.br
daguerra@ufpa.br
aguicruz@ufpa.br
fabiobaarros@gmail.com

Abstract. *This work deals with investigation of a turbulent impinging jet configuration from numerical simulation using hybrid equations employed by Shear-Stress Transport* (SST) $\kappa - \omega$ *. The jet goes out from a fully developed pipe flow at number Reynolds of 35000. To compare with the numerical results, the experimental data set of Guerra* et al. *(2005) is used to describe the full mean temperature and velocity profiles for the radial position along the impingement plate with circular nozzle. The effects of nozzle-to-plate spacing on the flow and heat transfer have been investigated. The velocity fields are well estimated by the simulation in the inner layer along the wall jet region. In particular, at the radial location* $r/D = 2$ *these profiles distributions exhibit little variance . This analysis yet revealed that a recirculation bubble supports the heat transfer.*

Keywords: *Impinging jet, turbulence, velocity profiles, heat transfer*

1. INTRODUCTION

Impinging jet flows have simple configuration geometry and provides a high heat transfer, but complex configuration of the flow dynamics appears after the flow impinging on the plate (Guerra *et al.*, 2005). Several studies have shown the nozzle-to-plate spacing influence and its correlation with the Nusselt number (see, e.g., Jambunathan *et al.* (1992); Anwarullah *et al.* (2012)). The main conclusion is that with large nozzle-to-plate spacing, the Nusselt Number is not strongly affected and that the heat transfer rate decrease.

The shape of the nozzle is considered to obtain a better heat transfer rate. Attalla *et al.* (2017) observed that the square nozzle shape compared to the circular one increase the heat transfer in about 10.7 $\%$. Further, both presents uniformity in the heat transfer with the increase of the Reynolds number. Zhao *et al.* (2004) have compared the circular nozzle to square, rectangular, and elliptical shapes using numerical simulation of the RNG $\kappa - \epsilon$ turbulent model. They observed that for dimensionless (H/D) nozzle-to-plate spacing from 2 to 4, non-circular nozzles presented better heat transfer rate compared to the circular nozzle. For nozzle-to-plate spacing over 5, the circular shape presented better performance.

The heat transfer of an impinging jet has a several studies for circular nozzle Grenson *et al.* (2016); Wu *et al.* (2016); Zargarabadi *et al.* (2018). Impinging jets generated from the motion of an oscillator exhibit the formation of vortex rings that increase thermal exchange with increasing nozzle-to-plate distance (see e.g., Greco *et al.* (2018)). He and Liu (2018) analyzes thermal exchange effects using circular and lobed nozzles, varying the space between plate and nozzle H/D = 2 and 4, at Reynolds number 10000. Using Large Eddy Simulation, the author noted that for distance H/D = 2 the wall region begin within the potential core of the free jet, however for H/D = 4 the development starts at the end of potential core.

The understanding of the fundamental physics of impinging jet flows, is often challenged by the large number of parameters that are needed to define the problem (J.B.R. Loureiro (2017)).Attention is often focused on the inlet geometry and flow conditions, the nozzle-to-plate spacing, the effects of Reynolds number, the role of vortical structures. The purpose of the present work is show up which phenomenon take places when a dimensionless (H/D) nozzle-to-plate parameter is changed and what provides high heat transfer rates. The present study is disposed conform to next steps. First, impinging jet flow configuration is presented (Section 2). Next the governing equations are discussed (Section 3). Following, the numerical methology is showed and validated against the experimental database (Section 4). To conclude, the data from the simulation are examed to obtain understanding related to the heat transfer process on the flat plate

(Section 5).

2. IMPINGING JET FLOW CONFIGURATION

In Figure 1 is shown a flow domain configuration of the turbulent impinging jet, cf. Czeslaw O. Popiel (1991). The flow presents complex regions on leaving the nozzle, namely: the free-jet region after leaving the nozzle, with ordered structures, initially laminar and not influenced by the target wall; the deflection region where the flow changes from axial to radial direction and the near wall region, where the boundary layer develops and the flow is turbulent.

Focus was given on the adjacent region of the flat surface, where the effects of turbulence dominates near the wall. The analysis of the impinging jet flow and heat transfer rates will be through the velocity and temperature fields. To validate the numerical results, the experimental data set of Guerra *et al.* (2005) was used to describe the mean temperature and velocity profiles at the wall jet region.

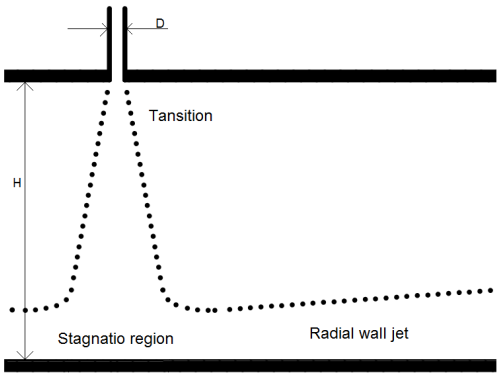

Figure 1: Impinging jet flow configuration.

The heat transfer rate on the surface of the impinging jet is described considering three fundamental parameters, namely, the convective exchange, boundary layer thicknesses, and the turbulence intensity. Zuckerman and Lior (2006). In this work, it was considered the thermal field into three regions (Katti and Prabhu, 2008), namely: a stagnation region, a transition region, and a wall jet region that extends over the radial direction (see illustration in Fig. 1).

3. GOVERNING EQUATIONS

The turbulent jet flow is described by solving the equations of continuity, momentum and energy:

$$\begin{aligned}
&\frac{\partial(\varrho u_i)}{\partial x_i} = 0, \\
&\frac{\partial(\varrho u_i u_j)}{\partial x_j} = -\frac{\partial P}{\partial x_i} + \frac{\partial}{\partial x_j}\left(\mu S_{ij} - \varrho\overline{u_i' u_j'}\right), \\
&\frac{\partial(\varrho C_p u_j T)}{\partial x_j} = \frac{\partial}{\partial x_j}\left(k\frac{\partial T}{\partial x_j} - \overline{\varrho C_p u_j' T'}\right).
\end{aligned} \tag{1}$$

In the Equations $(1)_{1,2}$, $\mathrm{S}_{ij} = \frac{1}{2}\left(\frac{\partial u_i}{\partial x_j} + \frac{\partial u_j}{\partial x_i}\right)$ is the axisymmetric part of the average velocity gradient tensor, the terms $\overline{u_i' u_j'}$ and $\overline{u_j' T'}$ are the turbulent tensors and the heat fluxes, respectively. Note that these terms were modeled as described in the next section.

To solve the closing problem of the turbulence was used the turbulent stress modeling Shear-Stress Transport (SST) $\kappa - \omega$, given by

$$\begin{aligned}
&\frac{\partial}{\partial x_i}(\rho\kappa u_i) = \frac{\partial}{\partial x_j}\left(\left(\mu + \frac{\mu_\tau}{\sigma_\kappa}\right)\frac{\partial}{\partial x_j}\right) + \widetilde{G}_\kappa - Y_\kappa + S_\kappa, \\
&\frac{\partial}{\partial x_i}(\rho\omega u_i) = \frac{\partial}{\partial x_j}\left(\left(\mu + \frac{\mu_\tau}{\sigma_\omega}\right)\frac{\partial}{\partial x_j}\right) + G_\omega - Y_\omega + D_\omega + S_\omega.
\end{aligned} \tag{2}$$

The model is associated by the definition of turbulent viscosity μ_t (see, e.g., Menter (1993))

$$\mu_t = \frac{\varrho\kappa}{\omega}\frac{1}{\max\left(\frac{1}{\alpha*}, \frac{S_{ij}F_2}{a_1\omega}\right)},$$
$$\omega = 10\frac{6(a_1\frac{\kappa}{S_{ij}})}{\beta_1(\Delta y)^2}, \qquad \kappa = \frac{1}{2}\overline{u_i'u_j'}. \tag{3}$$

Where κ is the turbulent kinect energy and ω is the rate of dissipation to the turbulent kinetic energy, a_1 and β_1 are constant, $\alpha*$ is the damping coefficient, F_2 is the blending function and y is the distance of next node to the wall.

In (2), the terms with index κ and ω refer to the turbulent kinetic energy and rate of dissipation, respectively. Thus, σ_κ and σ_ω are the turbulent Prandtl numbers, $\widetilde{G}_\kappa$ and G_ω are the mean generation of turbulence kinetic energy, Y_κ and Y_ω represent the dissipation due to turbulence, S_κ and S_ω represent source terms, and D_ω represents the cross-diffusion term (Fluent, 2015).

It is worthy to note that one of the advantages of SST $\kappa-\omega$ turbulent model is its relatively low computational cost for computing the turbulent viscosity μ_t.

The turbulent heat flux modeling is given by

$$\overline{u_i'T'} = -\frac{\nu_t}{\mathrm{Pr}_t}\frac{\partial T}{\partial x_i}, \tag{4}$$

where Pr_t is the turbulent Prandtl number, which relates the momentum diffusivity and the heat diffusivity, and ν_t is the kinematic turbulent viscosity.

The jet Reynolds number and instantaneous Nusselt number are defined as

$$Nu = \frac{q}{k}\frac{L}{\Delta T}, \qquad Re = \frac{\rho\overline{u}L}{\mu}, \tag{5}$$

where L is the length scale defined as the distance from the stagnation point. Herein, q, k, and ΔT are, respectively, the heat flux imposed to the surface, the thermal conductivity of the air, and the surface temperature difference.

4. NUMERICAL METHODOLOGY

The next part details the computational and the numerical domain. ANSYS FLUENT 16.0 finite volume computer code was used for the RANS simulation (Fluent, 2015). Based on a finite volume method it solves the Navier-Stokes equations in a cell-centered grid system. The coupling of the velocity and pressure is performed by the SIMPLE algorithm. For steady bi-dimensional convection, the discretization was through Second Order Upwind scheme (Patankar and Spalding (1983)). The least squares cell-based was used to check gradients and derivatives. The pressure scheme was PRESTO. To reduce the computational time, the $\kappa-\epsilon$ model by Jones and Launder (1972), was at first used in each mesh until convergence. Once the flow becomes fully converged the SST $\kappa-\omega$ model initialized. The experimental data of Guerra *et al.* (2005) was used to validate the results in present simulation.

4.1 Domain and boundary conditions

The computational domain of the study is shown in Fig. 2, the jet consists of a circular nozzle with $D = 43,5mm$, dimensionless (H/D) nozzle-to-plate spacing $H/D = 1$ and $H/D = 2$.The radial length is counter from the diameter jet center of the incidence region until to the plate edge at r=420mm. Note that the geometry of interest is symmetrical. Herein, the numerical calculations have been carried out for the entire flow domain.

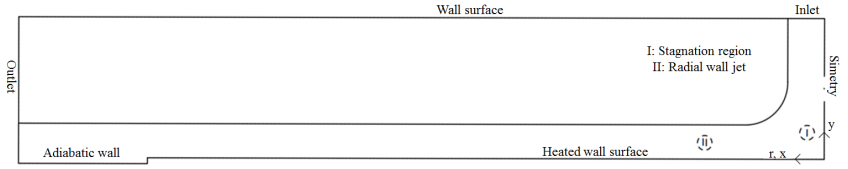

Figure 2: Computational domain and boundary conditions.

According to Guerra *et al.* (2005), the hydraulic diameter and the turbulent intensity are 0.0435 and 5%, respectively. The inlet conditions was performed separately from a circular duct using periodic boundary conditions since the actual state at the entrance to the experiment is fully developed flow. In the walls, the shear condition was non-slip. On the

impigiment flat surface was imposed a heat flux $Q = 284W/m^2$. The inlet fluid was fitted to $T_i = 297K$, ambient temperature. The air flow is assumed to be incompressible with the maximum velocity of 12 m/s at the inlet and the constant atmospheric pressure boundary condition was imposed at the outlet open boundaries.

4.2 Meshing strategy and solution control

In this analysis, Tab. 1 shows three different meshes that were tested, all with hexahedral elements and structured division. The grid used is described in Fig. 3a, the refinement was performed by increasing the number of elements as it approaches the impact region. Moreover, the turbulence model used required that the node closest to the wall be a distant $y^+ < 1$ inclusive for the coarser mesh (see Fig. 3b). Figure 4a shows the estimated effect of the Nusselt number on the flat plate for the three meshes. The coarse mesh solution predicts just on maximum peak in the stagnation region. From $0.05m$ when the development of the boundary layer begins there is a decrease of Nu. The fine mesh result shows two maximum peaks, due to high Reynolds number and vortices that break down from the shear layer according Dogruoz *et al.* (2015). Fig 4b demonstrate that this behavior was also observed skin friction , the fine and medium meshe showed a second peak closer to the stagnation region. It is observed that $y^+ = 0.577$, in the stagnation region, does not predict satisfactorily the behavior of Nu and C_f according Huang *et al.* (2018, 2019). A slight difference can be noticed between meshs two and three. For this reason, the grid resolution with 350 thousands cells is chosen with acceptable precision and lowest cost.

Meshs	Total size (thousand)	y^+
Fine: 3	500	0.295
Medium: 2	350	0.421
Coarse: 1	200	0.577

Table 1: Numerical grid resolution.

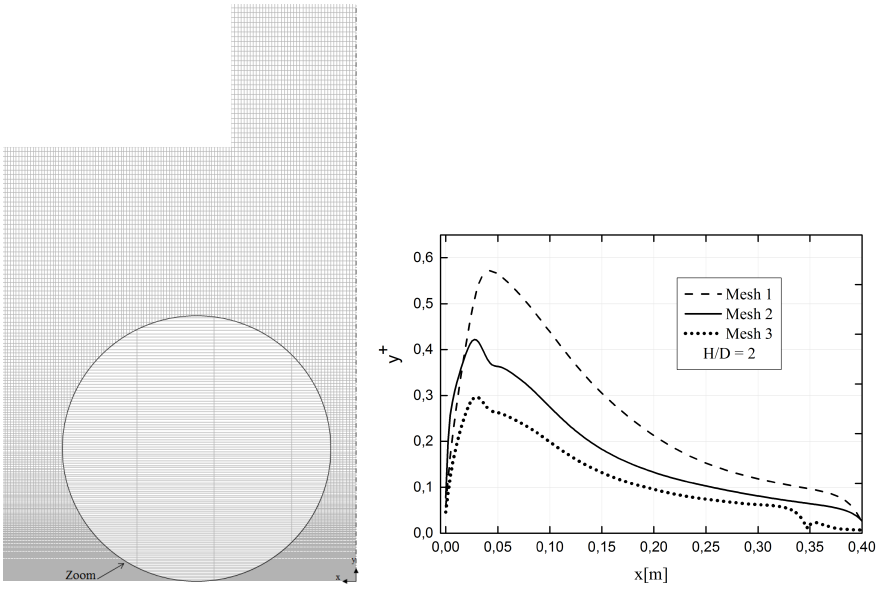

(a) Grid distribution.

(b) Effect the grid on y^+.

Figure 3: Mesh of the computational domain.

The flow throughout the domain have been monitored by residuals, to verify whether the equations were solved with accuracy. Celik *et al.* (2008) summarized that in a range of $1E^{-4} - 1E^{-5}$ there is good convergence and for the most part satisfactory to engineering applications. For all computations, was assumed to be converged after show up tiny oscilantions in velocity and temperature.

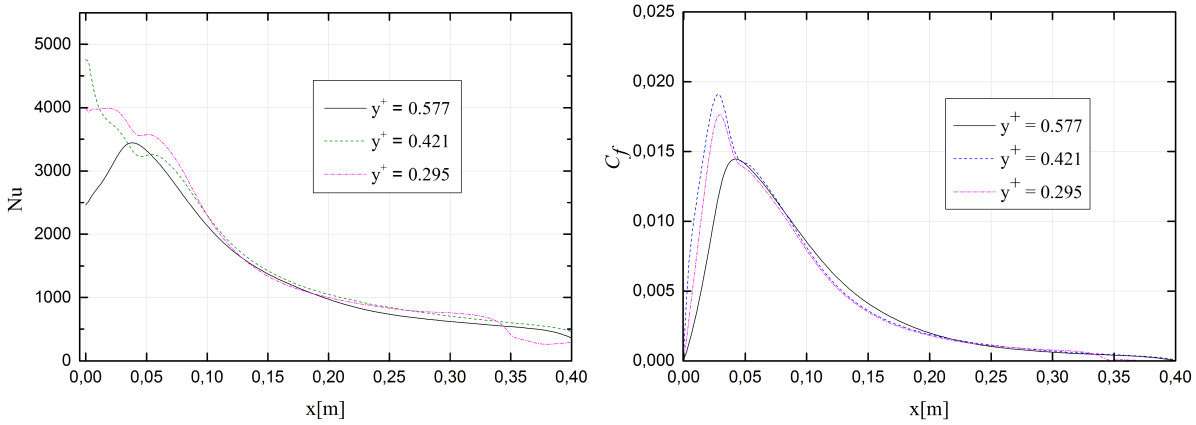

(a) Nulsselt number. (b) Skin friction.

Figure 4: The grid independence tests using three meshes for $H/D = 2$.

5. RESULTS AND DISCUSSION

The mean velocity profiles presented were obtained in the wall jet zone. The numerical data for Re = 35000 and H/D = 2 are shown in six different radial positions r = 80, 85, 90, 95, 100, and 105 mm, is validated against experimental data of Guerra *et al.* (2005).

The results for r = 80, 85, 90, 95 100, and 105 shown in Fig. 6 expresses the behavior of radial velocity $\langle u \rangle$ varying with distance $\langle y \rangle$ from the impingiment plate. The fact that, in the present case, the inner layer was calculated regarding $y^+ < 1$, Fig. 6 shows that the distribution of velocity profile agreed successfully with the experimental data for viscous sublayer. For the thermal case, it was observed that near the stagnation point the numerical values have large difference compared to the experimental ones. The velocity profiles, as the flow away from the impinging region, present a decrease in the average velocity values.

In order to relate the dimensionless (H/D) nozzle-to-plate spacing to the heat transfer, the recirculation zone in the wall jet region is analyzed. One reminds that are formed by the influence of the confine wall and can be interpreted as the increase in the difference pressure between the walls. From the observation of a recirculation bubble in velocity contour, a shear layer can be noted. Fig. 5 illustrates contours of velocity magnitude for H/D = 1 and 2. For smaller nozzle-to-plate reveal large recirculation zone, affecting zones more closest to the stagnation region producing an extension in this region. As well as notable raise on heat transfer.

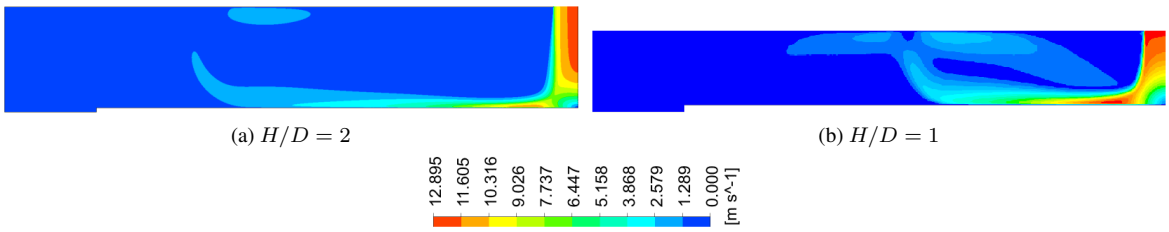

(a) $H/D = 2$ (b) $H/D = 1$

Figure 5: Contours of radial velocity; $Re = 35000$.

The temperature profiles had calculated for Re = 35000 and H/D = 2 at the same radial positions where the average velocity profiles were obtained. Validation of heat transfer performed in this study is shown in Fig. 7. For $80 \leq r \leq 100$, the numerical result reveals the trend of the shape thermal field, with a slight overestimation of the maximum temperature values. Region $80 \leq r \leq 85$ corresponds to the beginning zone of the boundary layer.The linear behavior ranging $0.005 \leq y \leq 0.015$ suggest the formation of a radial shear layer existing between the recirculation bubble and the boundary layer.

The present investigations at Reynolds number of 35000 for H/D =1 and 2, it is found that the recirculation bubble in radial distribution of flow fluid is appearing at $r \geq 80$ i.e. within the wall jet boundary layer. In this region the turbulent boundary layer becomes more influenced by shear boundary layer and the jet exit velocity is still present until $r \leq 115$. Moreover, results shown that the recirculation bubble affects velocity performance, is also the heat transfer. It is worth noting that the temperature profiles exhibits representative behabior of the thermal flow, despite of the fact that temperature field were underpredicted.

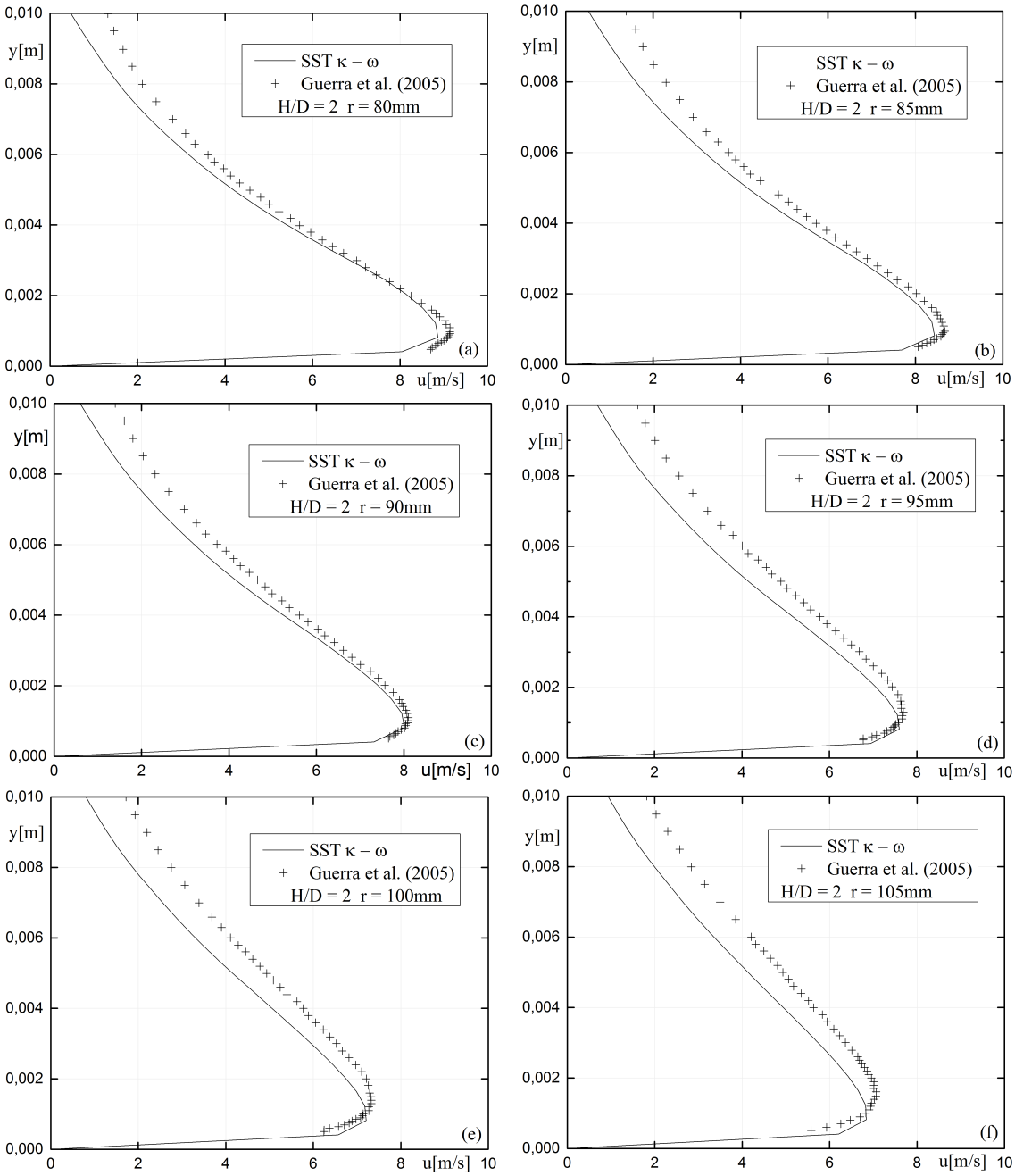

Figure 6: Distribution of radial velocity compared with Guerra *et al.* (2005) data for H / D = 2 at six radial positions (a) r = 80 mm, (b) r = 85 mm, (c) r = 90 mm, (d) r = 95 mm, (e) r = 100 mm, (f) r = 105 mm.

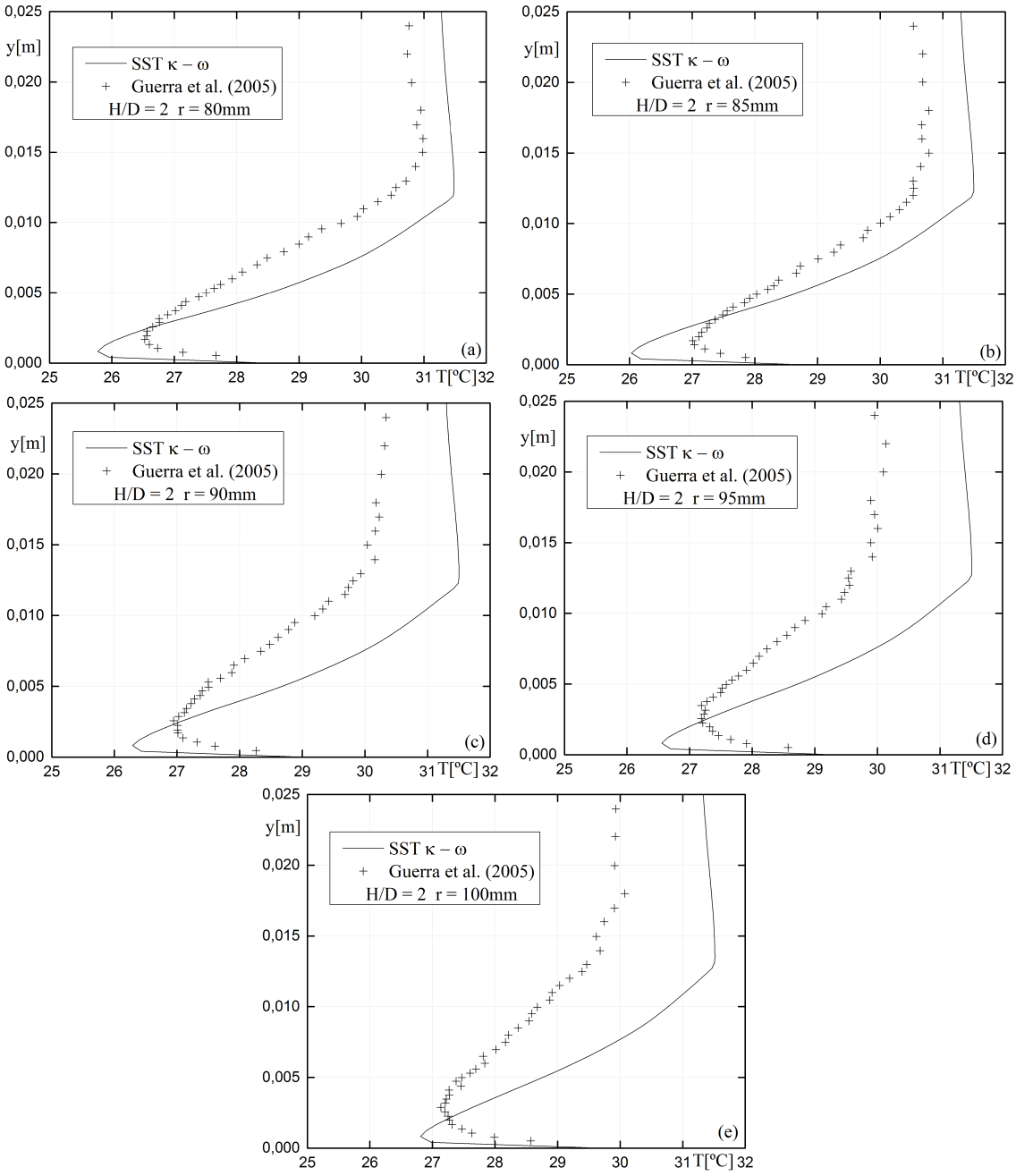

Figure 7: Temperature profiles in the radial positions.

6. CONCLUDING REMARKS

A SST $\kappa - \omega$ simulation of an impinging jet onto a heated flat surface has been performed at high Reynolds number. The simulation has been rightly validated on a experimental data base. It was predicted the flow dynamics and the heat transfer of a turbulent impinging jet considering nozzle-to-plate spacing, circular nozzle, and radial position along the impingement plate. The comprehensive data provided by this simulation permited to investigate what occur when the dimensionless (H/D) nozzle-to-plate spacing is changed. Based flow pattern, profiles of velocity and temperature profiles, the role played by recirculation zone on high convective heat transfer has been demonstrated. Only the recirculation bubble could be associated to increse on heat transfer rate. Furthermore, this phenomenon rebounds over all computational domain, not only in the radial wall jet. The understanding of flow behavior is however still incomplete and further investigation should be assumed to isolate the parameters that are responsible for the extension and/or intensification on heat transfer in the stagnation region.

As a first analysis, the numerical results predicted the flow behavior, however with unequal values. Was observed that the existence of a shear layer highly affect the Nusselt number distribution. The literature shows that maybe a core center and ring vortices lead a increases in the heat transfer in the stagnation zone. Therefore, to investigate this phenomenon, requests a finer mesh which will be the subject of a forthcoming paper.

7. REFERENCES

Anwarullah, M., Rao, V.V. and Sharma, K., 2012. "Effect of nozzle spacing on heat transfer and fluid flow characteristics of an impinging circular jet in cooling of electronic components". *Int. J. of Thermal & Environmental Engineering*, Vol. 4, No. 1, pp. 7–12.

Attalla, M., Maghrabie, H.M., Qayyum, A., Al-Hasnawi, A.G. and Specht, E., 2017. "Influence of the nozzle shape on heat transfer uniformity for in-line array of impinging air jets". *Applied Thermal Engineering*, Vol. 120, pp. 160–169.

Celik, I.B., Ghia, U., Roache, P.J. and Freitas, C.J., 2008. "Procedure for estimation and reporting of uncertainty due to discretization in cfd applications". *Journal of fluids Engineering-Transactions of the ASME*, Vol. 130, No. 7.

Czeslaw O. Popiel, O.T., 1991. "Visualization of a free and impinging round jet". *Experimental Thermal and Fluid Science*, Vol. 4, No. 3, pp. 253–264.

Dogruoz, M.B., Ortega, A. and Westphal, R.V., 2015. "Measurements of skin friction and heat transfer beneath an impinging slot jet". *Experimental Thermal and Fluid Science*, Vol. 60, pp. 213–222.

Fluent, A., 2015. "16.0, ansys fluent user's guide. ansys".

Greco, C.S., Paolillo, G., Ianiro, A., Cardone, G. and de Luca, L., 2018. "Effects of the stroke length and nozzle-to-plate distance on synthetic jet impingement heat transfer". *International Journal of Heat and Mass Transfer*, Vol. 117, pp. 1019–1031.

Grenson, P., Léon, O., Reulet, P. and Aupoix, B., 2016. "Investigation of an impinging heated jet for a small nozzle-to-plate distance and high reynolds number: An extensive experimental approach". *International Journal of Heat and Mass Transfer*, Vol. 102, pp. 801–815.

Guerra, D.R., Su, J. and Freire, A.P.S., 2005. "The near wall behavior of an impinging jet". *International journal of heat and mass transfer*, Vol. 48, No. 14, pp. 2829–2840.

He, C. and Liu, Y., 2018. "Large-eddy simulation of jet impingement heat transfer using a lobed nozzle". *International Journal of Heat and Mass Transfer*, Vol. 125, pp. 828–844.

Huang, H., Sun, T., Zhang, G., Li, D. and Wei, H., 2019. "Evaluation of a developed sst k-ω turbulence model for the prediction of turbulent slot jet impingement heat transfer". *International Journal of Heat and Mass Transfer*, Vol. 139, pp. 700–712.

Huang, H., Sun, T., Zhang, G., Sun, L. and Zong, Z., 2018. "Modeling and computation of turbulent slot jet impingement heat transfer using rans method with special emphasis on the developed sst turbulence model". *International Journal of Heat and Mass Transfer*, Vol. 126, pp. 589–602.

Jambunathan, K., Lai, E., Moss, M. and Button, B., 1992. "A review of heat transfer data for single circular jet impingement". *International journal of heat and fluid flow*, Vol. 13, No. 2, pp. 106–115.

J.B.R. Loureiro, A.S.F., 2017. "Velocity and temperature profiles, wall shear stress and heat transfer coefficient of turbulent impinging jets". *International journal of heat and mass transfer*, Vol. 107, pp. 846–861.

Jones, W. and Launder, B.E., 1972. "The prediction of laminarization with a two-equation model of turbulence". *International journal of heat and mass transfer*, Vol. 15, No. 2, pp. 301–314.

Katti, V. and Prabhu, S., 2008. "Experimental study and theoretical analysis of local heat transfer distribution between smooth flat surface and impinging air jet from a circular straight pipe nozzle". *International Journal of Heat and Mass Transfer*, Vol. 51, No. 17-18, pp. 4480–4495.

Menter, F., 1993. "Zonal two equation kw turbulence models for aerodynamic flows". In *23rd fluid dynamics, plasmadynamics, and lasers conference*. p. 2906.

Patankar, S.V. and Spalding, D.B., 1983. "A calculation procedure for heat, mass and momentum transfer in three-

dimensional parabolic flows". In *Numerical Prediction of Flow, Heat Transfer, Turbulence and Combustion*, Elsevier, pp. 54–73.

Wu, W., Banyassady, R. and Piomelli, U., 2016. "Large-eddy simulation of impinging jets on smooth and rough surfaces". *Journal of Turbulence*, Vol. 17, No. 9, pp. 847–869.

Zargarabadi, M.R., Rezaei, E. and Yousefi-Lafouraki, B., 2018. "Numerical analysis of turbulent flow and heat transfer of sinusoidal pulsed jet impinging on an asymmetrical concave surface". *Applied Thermal Engineering*, Vol. 128, pp. 578–585.

Zhao, W., Kumar, K. and Mujumdar, A., 2004. "Flow and heat transfer characteristics of confined noncircular turbulent impinging jets". *Drying Technology*, Vol. 22, No. 9, pp. 2027–2049.

Zuckerman, N. and Lior, N., 2006. "Jet impingement heat transfer: physics, correlations, and numerical modeling". *Advances in heat transfer*, Vol. 39, pp. 565–631.